Surface passivation of random alloy AlGaAsSb avalanche photodiode

Peng Cao,[1,2] Hongling Peng,[1,3] Tiancai Wang,[1,4] Vibha Srivastava,[5] Manoj Kesaria,[5] Minghui You,[6] Qiandong Zhuang,[7] and Wanhua Zheng[1,2,3,4,✉]

[1]*Laboratory of Solid-State Optoelectronics Information Technology, Institute of Semiconductors, Chinese Academy of Sciences, Beijing, China*
[2]*Center of Materials Science and Optoelectronics Engineering, University of Chinese Academy of Sciences, Beijing, China*
[3]*State Key Laboratory on Integrated Optoelectronics, Institute of Semiconductors, Chinese Academy of Sciences, Beijing, China*
[4]*School of Electronic, Electrical and Communication Engineering, University of Chinese Academy of Sciences, Beijing, China*
[5]*School of Physics and Astronomy, Cardiff University, Cardiff, UK*
[6]*Information Technology College, Jilin Agricultural University, Changchun, China*
[7]*Physics Department, Lancaster University, Lancaster, UK*

✉Email: whzheng@semi.ac.cn

AlGaAsSb attracts significant interest for near-infrared avalanche photodiodes (APD). The authors report a two-order reduction in the dark current and a six-time enhancement of gain in random alloy (RA) AlGaAsSb APD that is surface passivated by conformal coating of Al_2O_3 via atomic layer deposition (ALD). The dark currents of the APDs with 400-μm diameter (dry etched) at 90% breakdown voltage (0.9 V_{br}) are $(5.5 \pm 0.5) \times 10^{-5}$ A, $(2.1 \pm 0.4) \times 10^{-5}$ A, and $(6.2 \pm 0.8) \times 10^{-7}$ A for non-passivated, Si_3N_4 passivated, and Al_2O_3 passivated devices, respectively. The dark current at a gain of 10 for the Al_2O_3 passivated device is 1×10^{-8} A which is comparable to the reported value for 100-μm diameter mesa diodes passivated by SU-8. Maximum gain values of 6, 12, and 35 were obtained for non-passivated, Si_3N_4 passivated, and Al_2O_3 passivated devices, respectively. Moreover, punch-through capacitance of 8 pF in a spectral response of 450 to 850 nm was obtained. Thus, Al_2O_3 passivation can be the best solution for antimonide optoelectronic devices.

Introduction: Avalanche photodiodes (APD) play an important role in many important fields such as quantum optics, optical communication, light detection and ranging (LIDAR), surveillance, and molecule sensing [1–3]. The internal gain in APD improves the signal-to-noise ratio of a detector system and plays an important role in reducing the impact of the readout electronic noise. Silicon is an excellent material for APD for wavelengths below 1.0 μm. But for wavelengths above 1.0 μm, current commercial short wave infrared (SWIR) APD comprises SACM structure with separate (S), absorption (A), charge (C), and multiplication (M) regions. The performance of SACM APD is tailored by manipulating the absorber's and multiplier's properties. Commercial SACM APD are designed with a high gain due to the required of high electric field in the multiplication region (wide bandgap InAlAs or InP) and the low tunnelling dark current with low electric field in the absorber region (narrow bandgap material such as InGaAs). For the high-performance APDs ranging from 1.55 to 2.00 μm, the linear and Giger mode SACM APD with wide gap AlAsSb or AlGaAsSb in the multiplication region appear promising alternatives to InAlAs and InP. Recently, it is shown that AlGaAsSb as a multiplication region is gaining increasing attention due to its low excess noise and low k (the ratio of electron and hole impact ionization coefficients) of 0.01 compared to Si APDs (k_{Si}~0.01) [4, 5]. AlGaAsSb APDs operating in the range of 1.55 to 2.00 μm with InGaAs absorber demonstrates a high gain-bandwidth product [6, 7] and a small temperature coefficient of breakdown voltage for APDs with GaAsSb absorption layer [8, 9]. Also, APDs with thick digital alloy (DA) AlGaAsSb [4, 10] and random alloy (RA) AlGaAsSb [11, 12] were reported, where RA AlGaAsSb were superior in comparison to DA AlGaAsSb as they are easy to grow and manufacturable.

However, the passivation of this AlGaAsSb is not fully explored. The mesa sidewalls are usually with a SU-8 polymer [11]. There are no reports on the surface passivation of antimonide APD with Al_2O_3. This letter reports, for the first time, the surface passivation using Al_2O_3 for AlGaAsSb RA APD with 75% Al, in terms of dark current, photo response, and gain characteristics compared with devices that were non-passivated, Si_3N_4 and Al_2O_3 passivated. Significant reduction in dark current characteristic and improvement in gain value were presented. This work simplifies the passivation process with minimized degradation to the device materials for photodetectors containing RA AlGaAsSb.

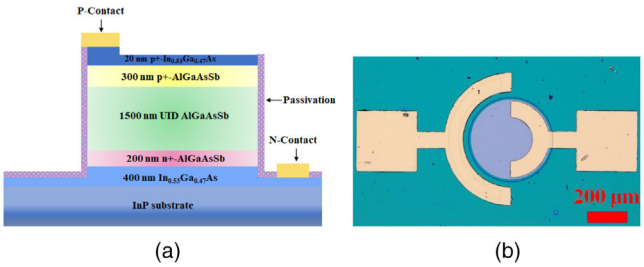

Fig. 1 *Schematic configuration of the AlGaAsSb APD device. (a) Cross section of mesa type APD device. (b) Microscope image of the APD device. APD, avalanche photodiodes.*

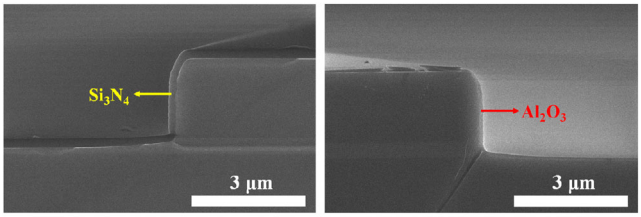

Fig. 2 *SEM images of sidewalls of mesa with a passivation layer of (a) Si_3N_4 and (b) Al_2O_3. SEM, scanning electron microscope.*

Device configuration and fabrication: The APD was grown by molecular beam epitaxy (MBE) on the InP substrate. It comprises a topmost 20-nm p-type $In_{0.53}Ga_{0.47}As$ layer (~1×10^{19} cm^{-3}), 300-nm p-type AlGaAsSb (~2×10^{18} cm^{-3}) layer, 1500-nm undoped AlGaAsSb, followed by a 200-nm n-type AlGaAsSb (~2×10^{18} cm^{-3}) and a 400-nm n-type $In_{0.53}Ga_{0.47}As$ (1×10^{19} cm^{-3}) buffer layer. All layers were grown at a temperature of ~ 450°C. The grown wafer was dry-etched into a 400-μm diameter mesa using Inductively Coupled Plasma (ICP), followed by deposition of Si_3N_4 by plasma-enhanced chemical vapour deposition (PECVD) or Al_2O_3 by atomic-layer deposition (ALD). Mesa devices without passivation were also fabricated as reference. The schematic configuration and the microscope image of the devices are shown in Figures 1a and 1b.

Figures 2a and 2b show the scanning electron microscope (SEM) image of the vertical sidewall of the mesa coated with Si_3N_4 and Al_2O_3. The images confirm the smooth vertical sidewalls and a conformal coating of the sidewalls with Si_3N_4 and Al_2O_3. The ALD-deposited Al_2O_3 is thinner than the PECVD-deposited Si_3N_4.

Figure 3 shows the measured capacitance–voltage (C–V) characteristic and the depletion width of the APD devices with a diameter of 400 μm. The capacitance value drops sharply from 0 to −5 V, and then saturates at −30 V. Meanwhile, the depletion width saturates at 1500 nm. This represents that the AlGaAsSb APD is completely depleted at −30 V. This relatively high initial capacitance can be attributed to the large mesa area. Thus, we used −30 V as the point of unity gain to calculate the gain value.

Figure 4 shows the spectral response at zero bias of non-passivated, Si_3N_4, and Al_2O_3 passivated APD. The cutoff wavelength of AlGaAsSb APD devices under three passivation conditions is around 850 nm which is consistent with the bandgap energy of the alloy. Moreover, the APDs show a peak photo response at 670 to 680 nm. The slight variation of the peak wavelength is attributed to the instability of the light source in the measurement.

Figures 5a and 5b compare current–voltage (IV) measured under dark conditions for 400-μm non-passivated, Si_3N_4, and Al_2O_3 passivated

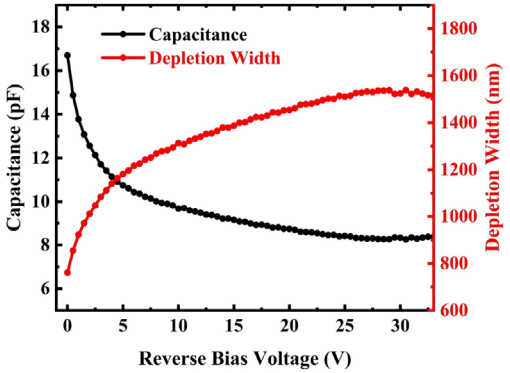

Fig. 3 *Measured C–V characteristic of APD devices at room temperature (300 K). APD, avalanche photodiodes.*

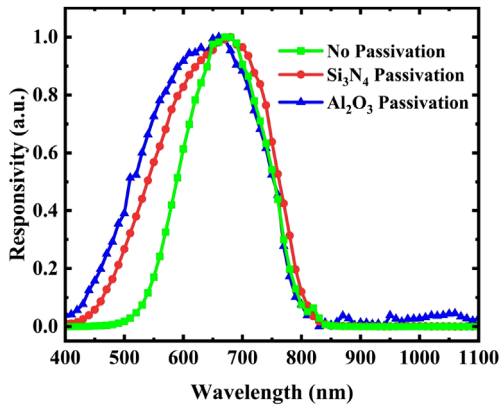

Fig. 4 *Spectral response of non-passivated and passivated AlGaAsSb APD at room temperature (300 K). APD, avalanche photodiodes.*

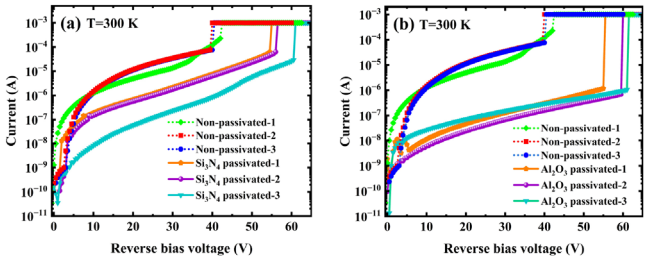

Fig. 5 *Dark current for the passivated and non-passivated AlGaAsSb APD at room temperature (RT). (a) Non-passivated devices and Si_3N_4 passivated devices. (b) Non-passivated devices and Al_2O_3 passivated devices. APD, avalanche photodiodes.*

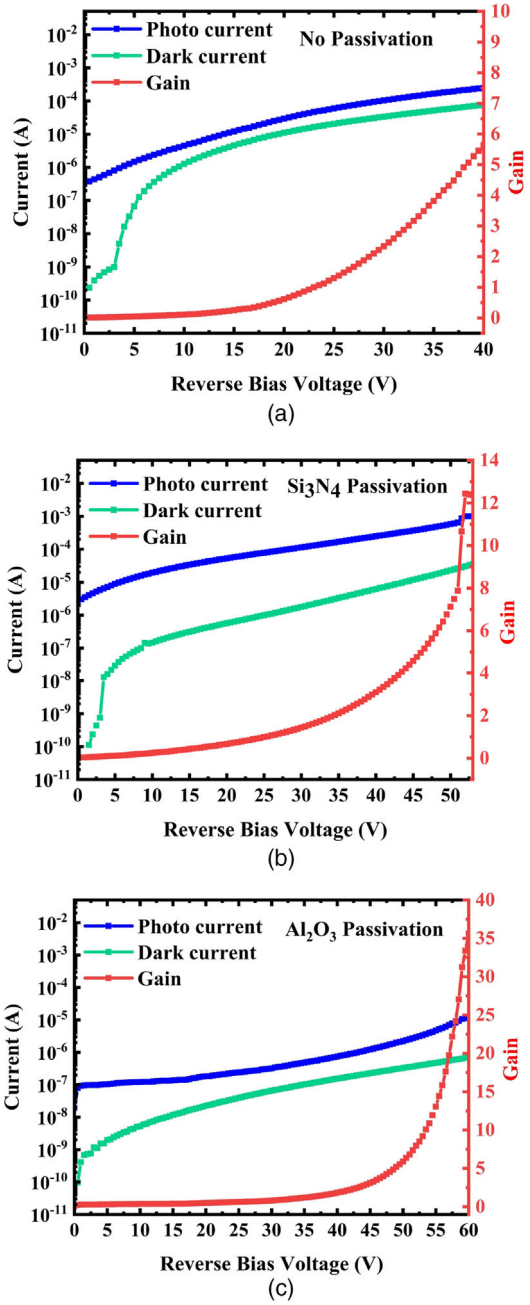

Fig. 6 *Photocurrent, dark current, and gain characteristic versus reverse bias: (a) non-passivated, (b) Si_3N_4, and (c) Al_2O_3 passivated APD at room temperature (300 K). APD, avalanche photodiodes.*

AlGaAsSb APD devices. Three devices have been measured for each type of passivation. The breakdown voltage (V_{br}) of non-passivated, Si_3N_4, and Al_2O_3 passivated devices are −40, −56.5, and −61 V, respectively, with dark current of $(5.5 \pm 0.5) \times 10^{-5}$, $(2.1 \pm 0.4) \times 10^{-5}$, and $(6.2 \pm 0.8) \times 10^{-7}$ A at 90% breakdown voltage (0.9 V_{br}) for the non-passivated, Si_3N_4 passivated, and Al_2O_3 passivated devices, respectively. The dark current density level of Al_2O_3 passivated device at 90% breakdown voltage is comparable to that of the SU-8 passivated AlGaAsSb APD device with a diameter of $D = 80$ μm [4]. It is worth noting that the dark current in our devices can be further suppressed by reducing the mesa size; hence, Al_2O_3 passivation offers a promising technique route to produce high-performance antimonide photodetectors. The reduction in dark current and the increased breakdown voltages for the passivated devices can be associated with an improved compensation of the residual dangling bonds and damages along mesa sidewalls processed by ICP etching. It should be noted that the presence of these defects causes surface leakage which results in an early breakdown, though the breakdown point associated with avalanche multiplication process in the active region remains the same for any surface passivation. The surface passivation suppresses surface leakage dominated breakdown, and as a consequence, it improves the breakdown voltage.

At 90% breakdown voltage, dark current is reduced by two orders of magnitude for Al_2O_3 passivation. The ALD-deposited Al_2O_3 is denser than the PECVD-deposited Si_3N_4. As a result, a relatively small fixed charge density reduces the chance of the band bending in the mesa sidewall. Moreover, intrinsic charges in Si_3N_4 provide a charge conduction channel of the sidewall, which could have deteriorated the dark current in Si_3N_4 compared to Al_2O_3 passivated APD [13].

Figures 6a to 6c show the photocurrent, dark current, and gain value versus reverse bias voltage for non-passivated and passivated APD. Based on Equation (1), the maximum gain values of 6, 12, and 35 are obtained for the non-passivated, Si_3N_4, and Al_2O_3 passivated APD, respectively. It has already been shown in Figure 5 that Al_2O_3 passivated APD devices present the best suppression effect of surface leakage current and hence surface breakdown. Thus, according to Equation (1), a gradual increase of photo and dark current for Al_2O_3 passivated devices was obtained before breakdown point compared to a sharp increase of photo current for the non-passivated and Si_3N_4 passivated devices (i.e.

the orders of magnitude difference of photo current between the point at unity gain and the point near breakdown for Al_2O_3 passivated APD devices are larger than the non-passivated and Si_3N_4 passivated cases), which correspondingly leads to the largest maximum gain value near breakdown for Al_2O_3 passivated APD devices.. We would like to highlight that the gain under the bias below the breakdown varies between the devices that were passivated differently, for example, $\sim$ 5.5, 3, and 2.5 for non-passivated, Si_3N_4 passivated, and Al_2O_3 passivated devices at a bias of -40 V. This can be associated with the different dependence of dark current and photo current on bias in terms of different passivation methods.

$$\text{Gain} = \frac{I_{ph} - I_d}{I_{ph0} - I_{d0}} \tag{1}$$

where I_{ph} and $I_d$stand for the photo and dark current at a certain voltage near breakdown point, while I_{ph0} and I_{d0} stand for the photo and dark current at the voltage slightly after the unity gain point.

Conclusion: In this work, optimal passivation conditions are obtained for AlGaAsSb APD. The dark current, photocurrent, photo response, and gain values of the non-passivated, Si_3N_4, and Al_2O_3 passivated APDs are compared. The APD devices under three passivation conditions reveal peak response wavelength of 670 to 680 nm. For the dark current characteristic, the Al_2O_3 passivated device represents a low dark current of $(6.2 \pm 0.8) \times 10^{-7}$ at 90% breakdown voltage while the dark currents are $(5.5 \pm 0.5) \times 10^{-5}$ A and $(2.1 \pm 0.4) \times 10^{-5}$ A for the non-passivated and Si_3N_4 passivated devices, respectively. Photocurrent was also measured and maximum gain values of 6, 12, and 35 were obtained for non-passivated devices, Si_3N_4 passivated devices, and Al_2O_3 passivated devices, respectively. This passivation investigation indicates that Al_2O_3 passivation of antimonide optoelectronic devices can help enhance their performance.

Author Contributions: Peng Cao: Conceptualization (lead); investigation (equal); formal analysis (lead); writing-original draft (lead). Hongling Peng: project administration (lead); writing-review and editing (supporting). Tiancai Wang: Formal analysis (supporting); investigation(equal). Vibha Srivastava: Methodology (supporting). Manoj Kesaria: Methodology (lead); Minghui You: Resources (supporting). Qiandong Zhuang: Resources (lead); writing-review and editing (lead). Wanhua Zheng: Funding acquisition (lead); supervision (lead).

Acknowledgements: This work is funded by the National Science and Technology Major Project of China (Grant No. 2018YFE0200900).

Author Contributions: Peng Cao: Conceptualization; Formal analysis; Investigation; Writing – original draft. Hongling Peng: Project administration; Writing – review & editing. Tiancai Wang: Formal analysis; Investigation. Vibha Srivastava: Methodology. Manoj Kesaria: Methodology. Minghui You: Resources. Qiandong Zhuang: Resources; Writing – review & editing. Wanhua Zheng: Funding acquisition; Supervision.

Conflicts of Interest Statement: The authors declare no conflict of interest.

Funding Information: This work is funded by the National Science and Technology Major Project of China (Grant No. 2018YFE0200900).

Data Availability Statement: The data that support the findings of this study are available from the corresponding author upon reasonable request.

doi: 10.1049/ell2.12956

References

1 Wang, F.-X., Wang, C., Chen, W., Wang, S., Lv, F.-S., He, D.-Y., Yin, Z.-Q., Li, H.-W., Guo, G.-C., Han, Z.-F.: Robust quantum random number generator based on avalanche photodiodes. *J. Lightwave Technol.* **33**(15), 3319–3326 (2015)

2 Song, B., Sun, J., Yan, Y., He, R., Zhou, X., Lu, W.: GM-APD lidar single-source data self-guided: Obtaining high-resolution depth map. *IEEE J. Sel. Top. Appl. Earth Obs. Remote Sens.* **16**, 4658–4669 (2023)

3 Gyongy, I., Davies, A., Gallinet, B., Dutton, N.A.W., Duncan, R.R., Rickman, C., Henderson, R.K., Dalgarno, P.A.: Cylindrical microlensing for enhanced collection efficiency of small pixel spad arrays in single-molecule localisation microscopy. *Opt Express* **26**(3), 2280–2291 (2018)

4 Lee, S., Kodati, S.H., Guo, B., Jones, A.H., Schwartz, M., Winslow, M., Grein, C.H., Ronningen, T.J., Campbell, J.C., Krishna, S.: Low noise Al0.85Ga0.15As0.56Sb0.44 avalanche photodiodes on InP substrates. *Appl. Phys. Lett.* **118**(8), 081106 (2021)

5 Grzesik, M., Donnelly, J., Duerr, E., Manfra, M., Diagne, M., Bailey, R., Turner, G., Goodhue, W.: Impact ionization in AlxGa1−XAsySb1-y avalanche photodiodes. *Appl. Phys. Lett.* **104**(16), 162103–162103-4 (2014)

6 Xie, S., Zhou, X., Zhang, S., Thomson, D.J., Chen, X., Reed, G.T., Ng, J.S., Tan, C.H.: InGaAs/AlGaAsSb avalanche photodiode with high gain-bandwidth product. *Opt Express* **24**(21), 24242–24247 (2016)

7 Abdullah, S., Tan, C.H., Zhou, X., Zhang, S., Pinel, L., Ng, J.S.: Investigation of temperature and temporal stability of AlGaAsSb avalanche photodiodes. *Opt. Express* **25**(26), 33610–33616 (2017)

8 Cao, Y., Blain, T., Taylor-Mew, J.D., Li, L., Ng, J.S., Tan, C.H.: Extremely low excess noise avalanche photodiode with GaAsSb absorption region and AlGaAsSb avalanche region. *Appl. Phys. Lett.* **122**(5), 051103 (2023)

9 Cao, Y., Osman, T., Clarke, E., Patil, P.K., Ng, J.S., Tan, C.H.: A GaAsSb/AlGaAsSb avalanche photodiode with a very small temperature coefficient of breakdown voltage. *J. Lightw. Technol.* **40**(14), 4709–4713 (2022)

10 Yi, X., Xie, S., Liang, B., Lim, L.W., Cheong, J.S., Debnath, M.C., Huffaker, D.L., Tan, C.H., David, J.P.R.: Extremely low excess noise and high sensitivity AlAs0.56Sb0.44 avalanche photodiodes. *Nat. Photonics* **13**(10), 683–686 (2019)

11 Lee, S., Guo, B., Kodati, S.H., Jung, H., Schwartz, M., Jones, A.H., Winslow, M., , Ronningen, T.J., Campbell, J.C., Krishna, S.: Random alloy thick AlGaAsSb avalanche photodiodes on InP substrates. *Appl. Phys. Lett.* **120**(7), 071101 (2022)

12 Kodati, S.H., Lee, S., Guo, B., Jones, A.H., Schwartz, M., Winslow, M., Pfiester, N.A., Grein, C.H., Ronningen, T.J., Campbell, J.C., Krishna, S.: AlInAsSb avalanche photodiodes on InP substrates. *Appl. Phys. Lett.* **118**(9), 091101 (2021)

13 Xu, X.-Y., Jiang, J.-K., Chen, W.-Q., Cui, S.-N., Zhou, W.-G., Li, N., Chang, F.-R., Wang, G.-W., Xu, Y.-Q., Jiang, D.-W., Wu, D.-H., Hao, H.-Y., Niu, Z.-C.: Wet etching and passivation of GaSb-based very long wavelength infrared detectors. *Chin. Phys. B* **31**(6), 068503 (2022)